Hydrodynamic Lubrication of Micro-Grooved Gas Parallel Slider Bearings with Parabolic Grooves

Yanjun LU*,**, Fuxi LIU***, Yongfang ZHANG****

*Xi'an University of Technology, Key Laboratory of Manufacturing Equipment of Shananxi Province, Xi'an 710048, China, E-mail: yanjunlu@xaut.edu.cn
**Huazhong University of Science and Technology, State Key Laboratory of Digital Manufacturing Equipment and Technology, Wuhan 430074, China, E-mail: yanjunlu@xaut.edu.cn
***Xi'an University of Technology, School of Mechanical and Precision Instrument Engineering, Xi'an 710048, China, E-mail: liufx28@163.com (corresponding author)
****Xi'an University of Technology, School of Printing, Packaging Engineering and Digital Media Technology, Xi'an 710048, China, E-mail: zhangyf@xaut.edu.cn (corresponding author)

1. Introduction

Opening micro-grooves in the surface of a mechanical component is thought to be an effective method for enhancing the performance of a mechanical component, such as a cylinder liner [1], piston ring [2], thrust bearing [3], journal bearing [4], or slider bearing [5]. In recent years, several theoretical and experimental studies concerning micro-grooved mechanical components have been conducted. Ali et al. [6] theoretically investigated the effect of micro-grooves on friction behaviour under elastohydrodynamic lubrication point contacts and established a good agreement with the experimental results. Yuan et al. [7] investigated the effect of groove orientation on sliding friction. The experimental results showed that grooves parallel or perpendicular to the sliding direction have an important influence on sliding friction. Experimentally, Zum Gahr et al. [8] examined the film thickness and friction coefficient of a micro-grooved oil-lubricated ceramic/steel friction pair. It was observed that grooves perpendicular to the sliding direction have the ability to generate a greater film thickness and lower friction coefficient than those parallel to the sliding direction. Luo et al. [9] used a unidirectional ball-on-disk sliding wear tester to study the wear resistance of micro-grooved surfaces, which demonstrated that the wear mass loss of micro-grooved surfaces generally increases as the groove spacing varies from 100 μm to 1000 μm. To improve the cutting performance, Obikawa et al. [10] applied a photolithography process to fabricate micro-grooves in the cutting tool surface. It was revealed that the presence of micro-grooves could reduce the friction force and friction coefficient. When the real topography of the cylinder liner was considered, Mezghani et al. [11] presented a friction model to investigate the friction performance of a micro-grooved piston ring-cylinder liner combination. They showed that the friction coefficient of the piston ring-cylinder liner combination could decrease by optimizing the geometric parameters of the micro-grooves. Kango et al. [12] investigated the steady-state performance of micro-grooved oil-lubricated hydrodynamic journal bearings. Du et al. [13] investigated the load performance of micro-grooved aerostatic journal bearings. Opening micro-grooves in the bearing surface could increase the load-carrying capacity in both of the studies. To analyze the hydrodynamic lubrication property of micro-grooved oil-lubricated parallel slider bearings, Shi and Ni [14] established a two-dimensional computational fluid dynamics simulation model. It was found that both load-carrying capacity and friction force increase as the sliding speed increased, and load-carrying capacity increases faster than friction force.

The effect of micro-grooves on hydrodynamic pressure has been systematically analyzed for micro-grooved oil-lubricated parallel slider bearings [14, 15]. However, no investigations detailing the effect of micro-grooves on hydrodynamic pressure seem to exist in the available literature for micro-grooved gas parallel slider bearings. Micro-grooved gas parallel slider bearings and micro-grooved oil-lubricated parallel slider bearings have different Reynolds equations. Therefore, investigating the hydrodynamic pressure of micro-grooved gas parallel slider bearings is necessary. In a previous investigation, Fu et al. [15] have employed parabolic grooves to evaluate the effects of minimum film thickness, groove width, depth, spacing, and orientation angle on the hydrodynamic pressure of micro-grooved oil-lubricated parallel slider bearings. In the present investigation, parabolic grooves are also employed to evaluate the hydrodynamic pressure of micro-grooved gas parallel slider bearings, and special attention is paid to the effects of sliding speed, groove width, depth, spacing, and orientation angle on average pressure.

2. Theory

Fig. 1 shows a schematic diagram of micro-grooved gas parallel slider bearings; the lower slider is grooved and fixed, the upper slider is smooth and moves along the x direction, the speed of the upper slider is U, the minimum film thickness between the two sliders is c and each groove has a depth of h_g.
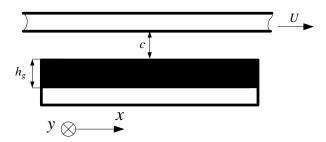
Fig. 2 shows the geometric model of a micro-grooved slider, where x and y are the coordinates in a global Cartesian coordinate system, l is the slider length, θ is the groove orientation angle, w_g is the groove width, s_g is the groove spacing, and l_g is the distance between two adjacent grooves.
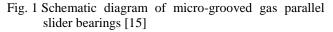
The upper slider and lower slider are separated by

the gas and the bearing works under the steady-state condition. The lubricant is a Newtonian fluid and the gas flow is isothermal and laminar. Hence, the compressible Reynolds equation for micro-grooved gas parallel slider bearings is expressed by:

$$\frac{\partial}{\partial x}\left(ph^3\frac{\partial p}{\partial x}\right)+\frac{\partial}{\partial y}\left(ph^3\frac{\partial p}{\partial y}\right)=6\mu U\frac{\partial(ph)}{\partial x}, \qquad (1)$$

where h is the gas-film thickness, p is the gas-film pressure, and μ is the fluid viscosity.

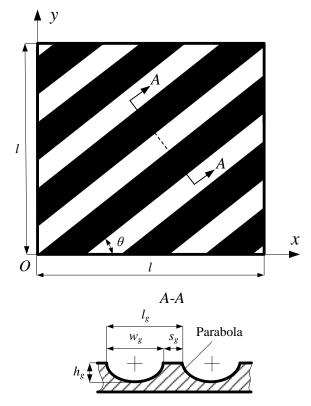Fig. 1 Schematic diagram of micro-grooved gas parallel slider bearings [15]

Fig. 2 Geometric model of a micro-grooved slider [15]

The dimensionless variables are defined as follows:

$$X=x/w_0,\ Y=y/w_0,\ P=p/p_a,\ H=h/c, \qquad (2)$$

where w_0 is the referenced groove width and p_a is the ambient pressure.

By submitting Eq. (2) into Eq. (1), the dimensionless Reynolds equation is obtained by:

$$\frac{\partial}{\partial X}\left(PH^3\frac{\partial P}{\partial X}\right)+\frac{\partial}{\partial Y}\left(PH^3\frac{\partial P}{\partial Y}\right)=\Lambda\frac{\partial(PH)}{\partial X}, \qquad (3)$$

where $\Lambda=6\mu Uw_0/(p_ac^2)$ is the bearing number.

The dimensionless gas-film thickness H is determined by the groove orientation angle θ. In the case of $0°\le\theta<90°$, the dimensionless gas-film thickness H is given by [15]:

$$H(X,Y)=\begin{cases}1+H_g-\dfrac{4H_g}{W_g^2}\left[\dfrac{(X\ tan\theta-Y)cos\theta-}{n_1L_g-\dfrac{1}{2}W_g}\right]^2,\\ \qquad Y<X\ tan\theta\ \text{and}\ Y_1<Y<Y_2\\[4pt] 1+H_g-\dfrac{4H_g}{W_g^2}\left[\dfrac{(Y-X\ tan\theta)cos\theta-}{n_1L_g-S_g-\dfrac{1}{2}W_g}\right]^2,\\ \qquad Y>X\ tan\theta\ \text{and}\ Y_3<Y<Y_4\\[4pt] 1,\quad \text{elsewhere}\end{cases}$$

$$\left.\begin{aligned}Y_1&=X\ tan\theta-(n_1L_g+W_g)\ sec\theta\\ Y_2&=X\ tan\theta-n_1L_g\ sec\theta\\ Y_3&=X\ tan\theta+(n_1L_g+S_g)\ sec\theta\\ Y_4&=X\ tan\theta+(n_1+1)L_g\ sec\theta\end{aligned}\right\}, \qquad (4)$$

while in the case of $\theta=90°$, the dimensionless gas-film thickness H is given by [15]:

$$H(X,Y)=\begin{cases}1+H_g-\dfrac{4H_g}{W_g^2}\left[\dfrac{X-n_2L_g-}{\dfrac{1}{2}W_g}\right]^2,\\ \qquad n_2L_g<X<n_2L_g+W_g\\[4pt] 1,\quad \text{elsewhere}\end{cases} \qquad (5)$$

where $n_1=fix\left|(X\tan\theta-Y)\cos\theta/L_g\right|$, $n_2=fix\left|X/L_g\right|$, fix is a function returning a value towards the nearest integer, $H_g=h_g/c$ is the dimensionless groove depth, $S_g=s_g/w_0$ is the dimensionless groove spacing, $W_g=w_g/w_0$ is the dimensionless groove width, and $L_g=l_g/w_0$ is the dimensionless distance between two adjacent grooves.

The boundary conditions of Eq. (3) are expressed by:

$$P(0,Y)=P(L,Y)=P(X,0)=P(X,L)=1, \qquad (6)$$

where $L=l/w_0$ is the dimensionless slider length.

The multi-grid finite element method solves Eq. (3), obtaining the dimensionless pressure P. The solution procedure for the multi-grid finite element method is that the algebraic equations formed by the finite element method are in turn smoothed by the interpolation from the

coarse grids to the fine grids and the restriction from the fine grids to the coarse grids, which is the finite Newton-Raphson iteration. In the present investigation, a multi-grid W-cycle and the finest grids with 1025×1025 nodes are adopted, where the number of the layers of the W-cycle is 4. The multi-grid finite element method is implemented using the MATLAB software. More detailed discussions regarding the multi-grid finite element method could be found in Liu et al. [4]. The converging condition is expressed by:

$$\left| P_{i,j}^{(1)} - P_{i,j} \right| \le 10^{-10}, \tag{7}$$

where $i = 1, 2,..., n_x$, $j = 1, 2,..., n_y$, n_x and n_y are the numbers of nodes in the x and y direction, respectively, $P_{i,j}$ is the dimensionless pressure at the point (i, j), and $P_{i,j}^{(1)}$ is the next dimensionless pressure of Newton-Raphson iteration.

The dimensionless average pressure P_{av} is given by:

$$P_{av} = \frac{p_{av}}{p_a} = \frac{\int_0^L \int_0^L P dX dY}{L^2}. \tag{8}$$

3. Results and discussions

Once investigating the average pressure of micro-grooved gas parallel slider bearings, some calculation parameters are constant: $l = 2.5$ mm, $p_a = 0.101325$ MPa, $\mu = 1.8 \times 10^{-5}$ Pa·s, $w_0 = 0.05$ mm, and $c = 3 \times 10^{-4}$ mm.

Fig. 3 shows the dimensionless gas-film pressure distributions over the slider surface in the case of $\theta = 30°$ and $\theta = 60°$. It is noted that the hydrodynamic pressure distribution is significantly affected by the geometric parameters of the grooves, closely correlating with the orientation angle. For both cases, the hydrodynamic pressure behaviours are similar and the optimum hydrodynamic pressure values are reached at the end of convergence clearance. However, the maximum pressure for $\theta = 60°$ is larger than that for $\theta = 30°$. Because there is no hydrodynamic lubrication effect for smooth gas parallel slider bearings, the values of the dimensionless pressure and dimensionless average pressure of smooth gas parallel slider bearings are both equal to 1. When compared with smooth gas parallel slider bearings, the maximum pressures in the cases of $\theta = 30°$ and $\theta = 60°$ are increased by approximately 24.6% and 41.6%, respectively.

In order to better demonstrate the effect of orientation angle θ on hydrodynamic pressure, Fig. 4 shows the dimensionless gas-film thickness distribution and dimensionless gas-film pressure distribution along the X direction at $Y = 25$. It is observed that the maximum pressure produced by each groove could be found near the right side of the groove along the X direction and is greatly affected by the orientation angle. The reason for this phenomenon could be explained by the fact that the right side of the groove is the end of convergence clearance and the orientation angle obviously controls the resistance of fluid influx. The results correlate with those obtained by Fu et al. [15].

Fig. 5 shows the effect of orientation angle θ on dimensionless average pressure at various values of dimensionless groove depth H_g. The average pressure increases with the increase of orientation angle when $H_g = 4$, 6, and 8. However, there is an optimum orientation angle to maximize the average pressure when $H_g = 2$, 4, 6, and 8. This optimum value is independent of the groove depth and equal to $90°$. Moreover, the number of the grooves for $\theta = 90°$ is smallest when $0° < \theta \le 90°$. The results imply that the average pressure is greatly affected by the number of the grooves.
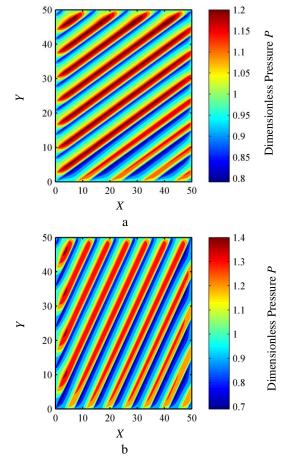
Fig. 3 Dimensionless gas-film pressure distributions for: (a) $\theta = 30°$ and (b) $\theta = 60°$ ($W_g = 4$, $S_g = 2$, $H_g = 4$, and $U = 6$ m/s)

Fig. 6 presents the effect of dimensionless groove depth H_g on dimensionless average pressure for different values of dimensionless groove width W_g. With the increase of dimensionless groove depth, the dimensionless average pressure initially increases, reaches a maximum value, and then gradually decreases. This maximum value is dependent of the dimensionless groove width. The results show that the depth of the grooves should be limited in order to obtain the maximum dimensionless average pressure. The pneumatic hammer vibration [13] of the gas-film could be efficiently avoided by limiting the depth of

the grooves. The results coincide with those obtained by Fu et al. [15].

For different values of dimensionless groove spacing S_g, Fig. 7 shows the effect of dimensionless groove width W_g on dimensionless average pressure. The results indicate that there is an optimum groove width to maximize the average pressure for any given groove spacing. This optimum value is dependent of the groove spacing. The results differ from those obtained by Fu et al. [15], which may be explained by the fact that the groove width has a different effect on dimensionless average pressure for different lubricants. The present study uses a compressible lubricant, but Fu et al. [15] use an incompressible lubricant.
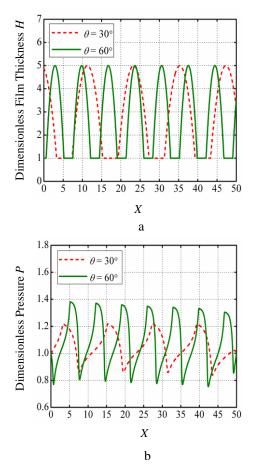

a

b

Fig. 4 (a) Dimensionless gas-film thickness distribution along the X direction at $Y = 25$; (b) dimensionless gas-film pressure distribution along the X direction at $Y = 25$ ($W_g = 4$, $S_g = 2$, $H_g = 4$, and $U = 6$ m/s)

Fig. 8 presents the effect of dimensionless groove spacing S_g on dimensionless average pressure for different values of dimensionless groove depth H_g. It is observed that the dimensionless average pressure generally increases as the dimensionless groove spacing varies from 1 to 46. Hence, the dimensionless average pressure is maximal when $S_g = 46$. The results show that the optimum dimensionless groove spacing for obtaining the maximum dimensionless average pressure is independent of the dimensionless groove depth. It is also observed that the

number of the grooves is equal to 1 when $S_g = 46$. These results and those obtained by Fu et al. [15] are not in agreement.
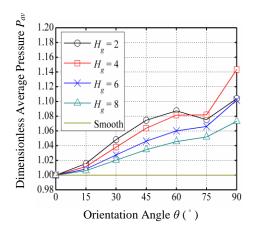

Fig. 5 Dimensionless average pressure P_{av} versus orientation angle θ for different values of dimensionless groove depth H_g ($W_g = 4$, $S_g = 2$, and $U = 6$ m/s)
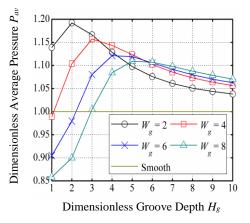

Fig. 6 Dimensionless average pressure P_{av} versus dimensionless groove depth H_g for different values of dimensionless groove width W_g ($\theta = 90°$, $S_g = 2$, and $U = 6$ m/s)
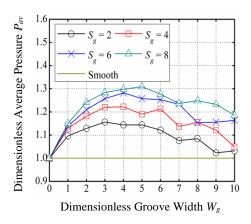

Fig. 7 Dimensionless average pressure P_{av} versus dimensionless groove width W_g for different values of dimensionless groove spacing S_g ($\theta = 90°$, $H_g = 4$, and $U = 6$ m/s)

Fig. 9 shows the effect of sliding speed U on dimensionless average pressure for different values of dimensionless groove depth H_g. The sliding speed has a different effect on average pressure for different groove depths. When $H_g = 2$ and 4 with increasing sliding speed, the average pressure initially increases, reaches a maximum value, and then gradually decreases. However, the average pressure increases with increasing sliding speed when $H_g = 6$ and 8. The results imply that the optimum sliding speed for maximizing the average pressure is dependent of the groove depth. Furthermore, there is an optimum value of groove depth to maximize the average pressure for any given sliding speed, and the value is dependent of the sliding speed. Therefore, an appropriate groove depth should be chosen according to the practical sliding speed in order to obtain the maximum average pressure.
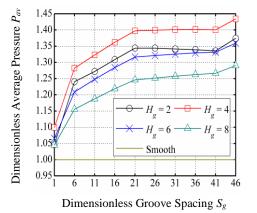

Fig. 8 Dimensionless average pressure P_{av} versus dimensionless groove spacing S_g for different values of dimensionless groove depth H_g ($\theta = 90°$, $W_g = 4$, and $U = 6$ m/s)
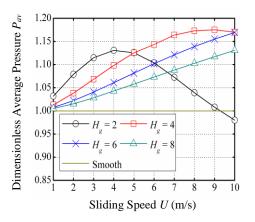

Fig. 9 Dimensionless average pressure P_{av} versus sliding speed U for different values of dimensionless groove depth H_g ($\theta = 90°$, $W_g = 4$, and $S_g = 2$)

4. Conclusions

A numerical study of micro-grooved gas parallel slider bearings with parabolic grooves is conducted. The following conclusions are made based on an analysis of the results:

1. The groove orientation angle controls the average pressure. Parabolic grooves should be perpendicular to the sliding direction in order to obtain the maximum average pressure.

2. The optimum groove depth for maximizing the average pressure is dependent of the groove width and the optimum groove width for maximizing the average pressure is dependent of the groove spacing. However, the optimum groove spacing for maximizing the average pressure is independent of the groove depth.

3. The sliding speed has a different effect on average pressure for different groove depths. Therefore, an appropriate groove depth should be chosen according to the practical sliding speed to obtain the maximum average pressure.

References

1. **Spencer, A.; Almqvist, A.; Larsson, R.** 2011. A numerical model to investigate the effect of honing angle on the hydrodynamic lubrication between a combustion engine piston ring and cylinder liner, IMechE Part J: Journal of Engineering Tribology 225(7): 683-689. http://dx.doi.org/10.1177/1350650111403867.

2. **Bouassida, H.; Biboulet, N.; Sainsot, P.; Lubrecht, A.A.** 2014. Piston ring load carrying capacity: influence of cross-hatching parameters, IMechE Part J: Journal of Engineering Tribology 228(6): 642-648. http://dx.doi.org/10.1177/1350650114522779.

3. **Papadopoulos, C.I.; Efstathiou, E.E.; Nikolakopoulos, P.G.** 2011. Geometry optimization of textured three-dimensional micro-thrust bearings, ASME Journal of Tribology 133(4): 041702-1-14. http://dx.doi.org/10.1115/1.4004990.

4. **Liu, F.X.; Lu, Y.J.; Zhang, Q.M.; Zhang, Y.F.; Gupta, P.; Müller, N.** 2016. Load performance analysis of three-pad fixing pad aerodynamic journal bearings with parabolic grooves, Lubrication Science 28(4): 207-220. http://dx.doi.org/10.1002/ls.1326.

5. **Rahmani, R.; Mirzaee, I.; Shirvani, A.; Shirvani, H.** 2010. An analytical approach for analysis and optimisation of slider bearings with infinite width parallel textures, Tribology International 43(8): 1551-1565. http://dx.doi.org/10.1016/j.triboint.2010.02.016.

6. **Ali, F.; Kaneta, M.; Křupka, I.; Hartl, M.** 2015. Experimental and numerical investigation on the behavior of transverse limited micro-grooves in EHL point contacts, Tribology International 84: 81-89. http://dx.doi.org/10.1016/j.triboint.2014.11.025.

7. **Yuan, S.H.; Huang, W.; Wang, X.L.** 2011. Orientation effects of micro-grooves on sliding surfaces, Tribology International 44(9): 1047-1054.

http://dx.doi.org/10.1016/j.triboint.2011.04.007.

8. **Zum Gahr, Z.H.; Wahl, R.; Wauthier, K.** 2009. Experimental study of the effect of microtexturing on oil lubricated ceramic/steel friction pairs, Wear 267: 1241-1251.
http://dx.doi.org/10.1016/j.wear.2008.12.108.

9. **Luo, K.Y.; Wang, C.Y.; Li, Y.M.; Luo, M.; Huang, S.; Hua, X.J.; Lu, J.Z.** 2014. Effects of laser shock peening and groove spacing on the wear behavior of non-smooth surface fabricated by laser surface texturing, Applied Surface Science 313: 600-606.
http://dx.doi.org/10.1016/j.apsusc.2014.06.029.

10. **Obikawa, T.; Kamio, A.; Takaoka, H.; Osada, A.** 2011. Micro-texture at the coated tool face for high performance cutting, International Journal of Machine Tools and Manufacture 51(12): 966-972.
http://dx.doi.org/10.1016/j.ijmachtools.2011.08.013.

11. **Mezghani, S.; Demirci, I.; Zahouani, H.; EI Mansori, M.** 2012. The effect of groove texture patterns on piston-ring pack friction, Precision Engineering 36(2): 210-217.
http://dx.doi.org/10.1016/j.precisioneng.2011.09.008.

12. **Kango, S.; Singh, D.; Sharma, R.K.** 2012. Numerical investigation on the influence of surface texture on the performance of hydrodynamic journal bearing, Meccanica 47(2): 469-482.
http://dx.doi.org/10.1007/s11012-011-9460-y.

13. **Du, J.J; Zhang, G.Q.; Liu, T.; To, S.** 2014. Improvement on load performance of externally pressurized gas journal bearings by opening pressure-equalizing grooves, Tribology International 73: 156-166.
http://dx.doi.org/10.1016/j.triboint.2014.01.012.

14. **Shi, X.; Ni, T.** 2011. Effects of grooves textures on fully lubricated sliding with cavitation, Tribology International 44(12): 2022-2028.
http://dx.doi.org/10.1016/j.triboint.2011.08.018.

15. **Fu, Y.H.; Ji, J.H.; Bi, Q.S.** 2012. Hydrodynamic lubrication of conformal contacting surfaces with parabolic grooves, ASME Journal of Tribology 134(1): 011701-1-9.
http://dx.doi.org/10.1115/1.4005518.

Yanjun Lu, Fuxi Liu, Yongfang Zhang

HYDRODYNAMIC LUBRICATION OF MICRO-GROOVED GAS PARALLEL SLIDER BEARINGS WITH PARABOLIC GROOVES

S u m m a r y

The hydrodynamic lubrication performance of micro-grooved gas parallel slider bearings with parabolic grooves is investigated in this paper. By using the multi-grid finite element method, the pressure distribution between a micro-grooved slider and a smooth slider is obtained. The geometric parameters of the parabolic grooves are optimized to maximize the average pressure under a given sliding speed. The numerical results show that geometric parameters such as groove depth, width, spacing, and orientation angle have an important influence on hydrodynamic pressure. Furthermore, the effect of sliding speed on hydrodynamic pressure is investigated under a given set of groove depths. It is observed that there is an optimum value of sliding speed to maximize the average pressure for any given groove depth and that the optimum value is dependent of the groove depth. The results of this study indicate that the average pressure could be improved by employing the optimized groove depth according to the practical sliding speed.